Topological Study of the Effect of the Isomorphic Substitution of Silicon by Aluminum on the Zeolite Structure and Its Interaction with Methane

N. B. Okulik

Departamento de Química, Facultad de Agroindustrias, UNNE. Cte. Fernández 755, 3700 Sáenz Peña, Chaco, Argentina

R. Pis Diez* and A. H. Jubert

CEQUINOR, Centro de Química Inorgánica (CONICET-UNLP), Departamento de Química, Facultad de Ciencias Exactas, UNLP, C.C. 962, B1900AVV La Plata, Argentina

The effect of the isomorphic substitution of silicon by aluminum on the structure of a zeolite cluster and its interaction with methane are studied within the framework of the density functional and the atoms-in-molecules theories. It is found that the inclusion of aluminum into the zeolite lattice leads to the development of Brønsted acid sites and to an increase in the base character of those oxygen atoms not involved in the acid sites. The calculated interaction energies indicate that methane interacts more strongly with the zeolite after the isomorphic substitution takes place, suggesting the importance of the Brønsted acid sites. The topological study clearly shows that the interaction of methane with the zeolite before the isomorphic substitution is dominated by a very weak Si−O···H−C van der Waals interaction. After the replacement of silicon by aluminum occurs, the interaction takes place through very weak Si−O···H−C and weak O−H···C van der Waals interactions, the latter being the main responsible for the stabilization of the complex.

Introduction

Zeolites are microporous inorganic compounds formed by corner-connected TO_4 (T = Si, Al) tetrahedral units. A lattice formed only by SiO_4 groups carries no electrical charge. The replacement of SiO_4 groups by AlO_4 units (also known as isomorphic substitution) induces negative charges in the lattice. The so-called Brønsted acid sites then appear when the negative charges are compensated by the formation of surface OH groups. Those acid sites are responsible for the catalytic behavior of zeolites.[1,2]

Both theoretical and experimental studies have been conducted to establish a relationship between the catalytic activity of zeolites and their structural and electronic properties, gas-phase acidity, and protonation energy among other properties. In particular, numerous calculations have been carried out on Brønsted acid sites in zeolites using clusters to represent the lattice within the framework of different methods and levels of theory.[3−14] It has been demonstrated that those methods based on the density functional theory (DFT)[15] constitute an excellent alternative to the more time-consuming post Hartree−Fock methods and are broadly effective for calculations using clusters to mimic zeolites.

The adsorption of hydrocarbons on zeolites is a process of interest both from empirical and theoretical viewpoints. Experimental data indicate that the adsorption energy of hydrocarbons on zeolites[16] is much smaller than the adsorption energy of small molecules with strongly polarized bonds.[2,17] By means of DFT calculations, Benco et al. show that the adsorption of linear hydrocarbons on zeolites containing only silicon atoms in the TO_4 units occurs through the formation of Si−O···H−C hydrogen bonds.[4] After the isomorphic substitution of Si by Al takes place, the hydrocarbon adsorption occurs via the formation of O−H···C hydrogen bonds involving the surface OH groups defining the Brønsted acid sites. The calculated adsorption energies indicate that the zeolite−hydrocarbon interaction is stronger in the second case.[4]

The isomorphic substitution of silicon by aluminum in a zeolite cluster constituted by three tetrahedrons is investigated in this work within the framework of the DFT and the atoms-in-molecules (AIM) theory developed by Bader and co-workers[18] to shed light on the effects of aluminum on the zeolite structure. Moreover, the interaction of methane with those clusters is also studied as a further step toward the understanding of the influence of the isomorphic substitution over the adsorption of hydrocarbons on zeolites.

Method and Calculation Details

The linear cluster constituted by three tetrahedrons (T3 from now on) has been used in numerous studies concerning the reactivity of Brønsted acid sites in zeolites and it is considered to provide a good description of the local properties of those sites,[5−7] especially in zeolites with high Si concentration as in the H-faujasite.[19]

The isomorphic substitution is simulated by replacing the Si atom in the midtetrahedron of the original T3 cluster containing three Si atoms by an Al atom. An additional hydrogen atom is then attached to a bridge O atom to form the acid site.

Those OH groups bound to the Si atoms in the terminal tetrahedrons are replaced by H atoms, the Si−H bond distance being fixed at 1.0 Å. This procedure not only simplifies the calculations but also avoids the presence of dangling bonds associated with the finiteness of the cluster model.

The optimized geometries of methane, the T3 clusters, and the adsorption products are obtained using Becke's three-parameter density functional[20] together with the gradient-corrected correlation density functional due to Lee, Yang, and Parr.[21] This combination leads to the well-known B3LYP method. The 6-311++G** basis set including both polarization

and diffuse functions is used throughout the work. All those calculations are accomplished with the Gaussian 98 package.[22] The geometry optimizations are carried out without any constraint, except for the Si−H distances mentioned above, which are kept fixed at 1.0 Å.

The interaction energies are calculated by subtracting the total energies of the reactants from the total energy of the product for each system under study. Thus, negative values of the interaction energy indicate stabilization when products are formed, whereas positive ones mean destabilization. The total energy of each reactant is computed by taking the basis set superposition error (BSSE) into account through the counterpoise method.[23] It must be stressed, nevertheless, that the interaction energies reported in this work should be taken as a qualitative trend of the reactivity pattern for each T3 model only. This is due to the presence of several imaginary frequencies that arise as a consequence of the Si−H bond distances, which remain fixed during geometry optimizations.

The topological study of the species under investigation in the present work is performed with the AIMPAC package[24] using electronic densities obtained at the 6-311++G**/B3LYP level of theory.

The AIM theory allows us to define the concepts of chemical structure and chemical reactivity in terms of the topological properties of the electronic density, $\rho(\mathbf{r})$.[18]

The formation of a chemical bond is the result of a competition between perpendicular contractions of $\rho(\mathbf{r})$ toward the bond path, leading to a charge density concentration along this line, and the parallel expansion of $\rho(\mathbf{r})$ away from the interatomic surface, yielding a charge density concentration within each atomic basin. The consequence of that behavior is the appearance of a critical point in $\rho(\mathbf{r})$ (bond critical point, BCP), at which the Hessian (or Laplacian) of $\rho(\mathbf{r})$ presents two negative eigenvalues (λ_1 and λ_2) and a positive one (λ_3). This means that $\rho(\mathbf{r})$ exhibits two negative curvatures perpendicular to the interatomic line and a positive one along the bond path. Calculated properties at the BCP of the electronic density are labeled with the subscript "b" throughout the work.

In the AIM theory atomic interactions are classified according to two limiting behaviors, namely, shared interactions and closed-shell interactions. Shared interactions are characteristic of covalent and polarized bonds and their main features are large values of ρ_b, $\nabla^2\rho_b < 0$, $|\lambda_1|/\lambda_3 > 1$, the quotient $G_b/\rho_b < 1$, G_b being the local kinetic energy density of the system evaluated at the BCP,[25] and $E_b < 0$, E_b being the local electronic energy density of the system calculated at the BCP and defined as the sum of the local kinetic energy density and the local potential energy density, V_b, both computed at the BCP.[18] In contrast, closed-shell interactions, useful to describe ionic bonds, hydrogen bonds, and van der Waals interactions, are characterized by small values of ρ_b, $\nabla^2\rho_b > 0$, $|\lambda_1|/\lambda_3 < 1$, $G_b/\rho_b > 1$, and $E_b > 0$.

The properties discussed above are presented in the following table for clarity and pedagogical issues

shared interactions large values of ρ_b	closed-shell interactions small values of ρ_b
$\nabla^2\rho_b < 0$	$\nabla^2\rho_b > 0$
$|\lambda_1|/\lambda_3 > 1$	$|\lambda_1|/\lambda_3 < 1$
$G_b/\rho_b < 1$	$G_b/\rho_b > 1$
$E_b < 0$	$E_b > 0$

Some other properties become very useful to characterize chemical bonds in general, including hydrogen bonds and van der Waals interactions in particular.
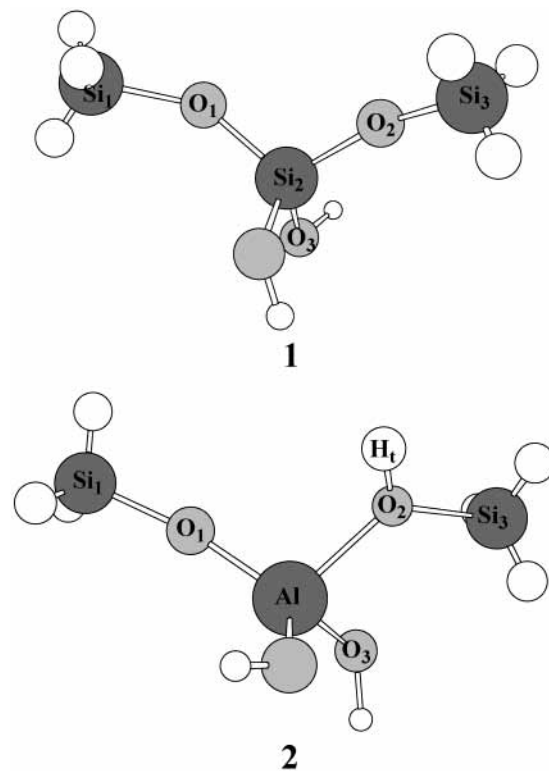

Figure 1. Optimized geometries of the isolated T3 clusters under study in the present work. See Table 1 for labels.

In the context of the AIM theory, the bonded radius of atom X, r_X, is defined as the distance from its nucleus to a BCP. In contrast, the van der Waals nonbonded radius of atom X, r°_X, is defined as the distance from the nucleus to a given value of its electronic density contour. The value 0.001 au is typically chosen because it corresponds to atomic sizes in molecules that are in good agreement with the van der Waals radii measured in gas-phase experiments.[26] It is said that an atom is penetrated when its bonded radius becomes smaller than its nonbonded radius, the extent of the penetration being measured by $\Delta r_X = r^\circ_X - r_X$. Furthermore, the mutual penetration of two atoms forming a chemical bond is obtained by adding the corresponding Δr's. It is found that the strength of the interaction between two atoms increases with their mutual penetration.[27]

Other properties are obtained by integrating the corresponding property density over the atomic basin, which is denoted by Ω.[18] The relevant atomic properties for the present work are the average number of electrons, $N(\Omega)$, from which the atomic net charge, $q(\Omega)$, can be calculated as $Z_\Omega - N(\Omega)$, Z_Ω being the nuclear charge of the atom; the atomic energy, $E(\Omega)$, the atomic volume, $V(\Omega)$, and the first moment of the atomic charge distribution, $M(\Omega)$, which measures the extent and direction of the dipolar polarization undergone by the atomic density.

Koch and Popelier used the above properties to establish a set of criteria to properly characterize hydrogen bonds.[28] Those criteria are used in the present work to study the interaction of methane with a T3 cluster before and after the isomorphic substitution of Si by Al.

Results and Discussion

Isomorphic Substitution of Si by Al. The optimized geometries of the clusters used to carry out the study proposed in the present work are shown in Figure 1. Table 1 summarizes the most relevant optimized geometrical parameters for those structures.

Effect of Si → Al Substitution on the Zeolite Structure

J. Phys. Chem. A, Vol. 107, No. 32, 2003 **6227**

TABLE 1: Selected Bond Lengths (r, Å) and Bond Angles (α, deg) of Optimized Geometries of Structures 1–4

parameter[a,b]	1	2	3	4
$r(Si_1-O_1)$	1.689	1.666	1.691	1.666
$r(T-O_1)$	1.619	1.711	1.620	1.714
$r(T-O_2)$	1.623	1.930	1.621	1.927
$r(T-O_3)$	1.659	1.749	1.656	1.757
$r(Si_3-O_2)$	1.685	1.768	1.685	1.766
$r(O_2-H_t)$		0.961		0.963
$r(C-H_a)$			1.091	1.092
$r(C-H_m)$			1.091	1.091
$r(O_1-H_a)$			2.913	3.392
$r(O_1-C)$			3.997	4.366
$r(O_2-C)$			3.993	3.465
$r(C-H_t)$				2.510
$\alpha(Si_1-O_1-T)$	147.7	170.0	146.0	166.3
$\alpha(O_1-T-O_2)$	109.1	104.0	109.0	103.9
$\alpha(T-O_2-Si_3)$	153.8	120.0	152.6	120.1
$\alpha(Si_3-O_2-H_t)$		118.7		118.9
$\alpha(H_m-C-H_a)$			109.8	108.8
$\alpha(O_1-H_a-C)$			172.6	149.3
$\alpha(O_2-H_t-C)$				169.6

[a] See Figures 1 and 4 for labels. [b] T is Si_2 in **1** and **3**. T is Al in **2** and **4**.

TABLE 2: Topological Properties (in au) of the Electronic Charge Density at Selected Bond Critical Points for Structures 1 and 2 (4 in Parentheses)[a]

bond[b,c]	ρ_b	$\nabla^2\rho_b$	$\|\lambda_1\|/\lambda_3$	G_b/ρ_b	E_b
Si_1-O_1	0.1135	0.7527	0.1706	1.9031	−0.0281
	(0.1220)	(0.8304)	(0.1696)	(1.9664)	(−0.0324)
$T-O_1$	0.1388	1.0035	0.1719	2.0944	−0.0397
	(0.0943)	(0.8241)	(0.1442)	(2.1124)	(0.0067)
$T-O_2$	0.1363	0.9884	0.1696	2.0902	−0.0378
	(0.0530)	(0.3751)	(0.1503)	(1.6453)	(0.0066)
$T-O_3$	0.1324	0.8555	0.1866	1.9313	−0.0418
	(0.0929)	(0.7521)	(0.1571)	(1.9849)	(0.0036)
Si_3-O_2	0.1138	0.7660	0.1692	1.9226	−0.0273
	(0.0961)	(0.5462)	(0.1818)	(1.6691)	(−0.0240)
O_2-H_t	−	−	−	−	−
	(0.3588)	(−2.5023)	(1.7025)	(0.1917)	(−0.6944)

[a] See Method and calculation details for an explanation of symbols. [b] See Figure 1. [c] T is Si_2 in **1**. T is Al in **2**.

It can be seen that the substitution of Si by Al leads to important changes in some of the geometrical parameters. The replacement of Si^{4+} by the larger Al^{3+} ion yields to the expected lengthening in the T−O bond distances. The $Si_3−O_2$ bond distance is also appreciably enlarged from structure **1** to structure **2**. This fact, however, can be related to the quasi-planar arrangement of the Al, H_t, and Si_3 atoms around the O_2 atom in structure **2**, thus leading to an sp^2-like hybridization scheme for this atom, although it is not clear from Figure 1. The $Si_1−O_1−T$ bond angle undergoes a significant increase from **1** to **2**, probably due to the larger radius of Al^{3+}. Finally, the $T−O_2−Si_3$ bond angle shows a decrease of more than 30° from structure **1** to structure **2**. It is worth noting that both the $Al−O_2−Si_3$ and $Si_3−O_2−H_t$ bond angles present values equal or very close to the *theoretical* value of 120°, a fact that seems to support the above argument concerning the sp^2-like hybridization scheme shown by O_2 in structure **2**.

Table 2 shows the topological properties calculated at different BCP's for structures **1** and **2**. It can be seen that all the Si−O and Al−O bonds are described by relatively small values of ρ_b, positive values of $\nabla^2\rho_b$, and large values of the G_b/ρ_b quotient. The local electronic energy density, E_b, presents very small values for those bonds, being both positive and negative. The $|\lambda_1|/\lambda_3$ quotient is always less than 1 for the Si−O and Al−O bonds. All these topological properties agree to
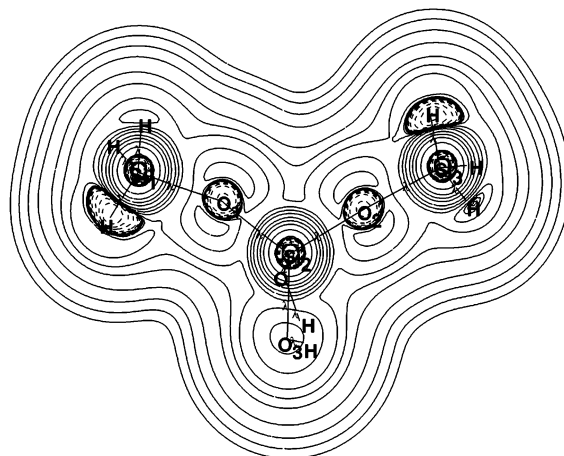

Figure 2. Laplacian of the electronic charge density of structure **1**. The plane containing the $Si_2−O_2−Si_3$ atoms is shown. Broken lines represent regions of electronic charge concentration, and solid lines denote regions of electronic charge depletion. BCP are indicated with black circles. The molecular graph is also indicated. The contours of the Laplacian of the electronic charge density increase and decrease from a zero contour in steps of $\pm 2 \times 10^n$, $\pm 4 \times 10^n$, and $\pm 8 \times 10^n$, with n beginning at −3 and increasing by unity. The same set of contours is used in all the figures of the present work.
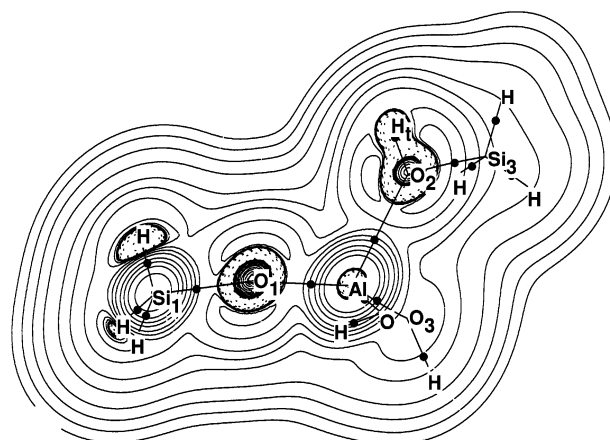

Figure 3. Laplacian of the electronic charge density of structure **2**. The plane containing the $Al−O_2−Si_3$ atoms is shown. Broken lines represent regions of electronic charge concentration and solid lines denote regions of electronic charge depletion. BCP are indicated with black circles. The molecular graph is also indicated.

characterize the Si−O and Al−O bonds as closed-shell interactions, that is, bonds in which ionic interactions are the dominant ones. On the other hand, the $O_2−H_t$ bond in structure **2** exhibits the essential features associated with the formation of shared interactions, namely, a relatively large value for ρ_b and a negative value for $\nabla^2\rho_b$. The $|\lambda_1|/\lambda_3$ quotient is appreciably greater than 1 and E_b is large and negative. Finally, the G_b/ρ_b quotient is less than 1. These topological properties clearly indicate that the $O_2−H_t$ bond that defines the Brønsted acid site is dominated by covalent, or slightly polarized, interactions.

Figures 2 and 3 show the $\nabla^2\rho(\mathbf{r})$ contour maps for structures **1** and **2**, respectively. It can be seen that the interaction pattern of Si and Al with the O atoms is nearly the same and clearly suggests the presence of interactions of the closed-shell type. On the contrary, the contour map of $\nabla^2\rho(\mathbf{r})$ exhibits a region of charge concentration along the $O_2−H_t$ bond, a characteristic feature associated with shared interactions.

Finally, the net charges, $q(\Omega)$, on O_1, O_2, and H_t are computed. It is found that the O_1 atom increases its negative

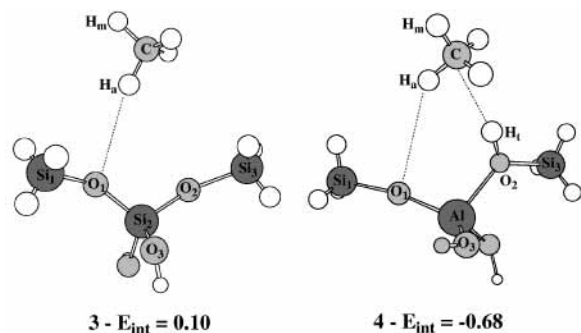**6228** *J. Phys. Chem. A, Vol. 107, No. 32, 2003*

Okulik et al.

Figure 4. Optimized geometries of the complexes formed between CH$_4$ and structures **1** and **2**, respectively. See Table 1 for labels. The interaction energies, in kcal/mol and corrected for the basis set superposition error, are also shown. Dashed lines indicate van der Waals interactions as found from the topological analysis.

net charge by about 0.04 au after the isomorphic substitution takes place. The O$_2$ atom, on the other hand, decreases its negative net charge by about 0.20 au, whereas the H$_t$ atom, not present in **1**, exhibits a net charge of about +0.40 au in **2**. These facts indicate that the isomorphic substitution of Si by Al on zeolites increases the base character of O$_1$ and allows the development of a Brønsted acid site formed by atoms O$_2$ and H$_t$.

Methane Adsorption onto the T3 Clusters. Figure 4 depicts the optimized structures of the complexes formed by the interaction of methane with structures **1** and **2**, respectively. The BSSE-corrected interaction energies are also shown in the figure. Table 1 reports the relevant optimized geometrical parameters of complexes **3** and **4**.

It can be seen that no appreciable changes occur in **1** and **2** as a result of the interaction with methane. On the other hand, the geometric parameters corresponding to the C—H bonds and H—C—H angles in methane are very similar to those found in the isolated molecule,[29] indicating that it is only slightly perturbed by the zeolitic systems. It can be seen from Table 1 that the O$_1$—H$_a$ distance is considerably shorter in **3** than in **4**. Moreover, the BSSE-corrected interaction energy for complex **3** is very small and positive, indicating that either a negligible or null interaction takes place between methane and cluster **1**. Thus, the small but negative BSSE-corrected interaction energy for complex **4** cannot be explained on the sole basis of a weak O$_1$—H$_a$ bond because it is weaker than the corresponding bond in **3**. It should be noted, on the other hand, that the O$_1$—C, O$_2$—C, and C—H$_t$ distances (the latter only in complex **4**) clearly show that methane moves toward the Brønsted acid site. The comparison of the value of the O$_1$—H$_a$—C bond angle in **3** and **4** supports that finding, too. It seems then that the slightly negative BSSE-corrected interaction energy for complex **4** could be attributed to a weak C—H$_t$ bond. These findings are in line with the results reported by Benco et al., who state that the adsorption of linear hydrocarbons on zeolites after the isomorphic substitution of Si by Al takes place occurs via the formation of O—H- - -C hydrogen bonds involving Brønsted acid sites.[4] Moreover, it is also interesting to see that Benco et al. reported a slightly negative interaction energy for methane with a purely siliceous structure (at a GGA level of theory).[4] Unfortunately, they show no results for the interaction of methane with a structure containing one acid site per cell. However, an extrapolation from C$_3$–C$_6$ data suggests an interaction energy of about 4–5 times greater than the value shown for the purely siliceous structure.[4] The calculations reported in the present work seem to follow the same trends that those provided by Benco et al.

TABLE 3: Topological Properties (in au) of the Electronic Charge Density at Selected Bond Critical Points for Structures 3 and 4 (4 in Parentheses)^a

bond^{b,c}	ρ_b	$\nabla^2\rho_b$	$|\lambda_1|/\lambda_3$	G_b/ρ_b	E_b
Si$_1$—O$_1$	0.1132	0.7471	0.1709	1.8966	−0.0279
	(0.1221)	(0.8278)	(0.1698)	(1.9615)	(−0.0326)
T—O$_1$	0.1386	0.9978	0.1723	2.0873	−0.0399
	(0.0938)	(0.8165)	(0.1443)	(2.1045)	(0.0067)
T—O$_2$	0.1371	0.9953	0.1698	2.0948	−0.0384
	(0.0535)	(0.3791)	(0.1510)	(1.6486)	(0.0066)
T—O$_3$	0.1324	0.8553	0.1894	1.9313	−0.0418
	(0.0886)	(0.7034)	(0.1571)	(1.9390)	(0.0040)
Si$_3$—O$_2$	0.1139	0.7673	0.1692	1.9236	−0.0274
	(0.0968)	(0.5519)	(0.1820)	(1.6752)	(−0.0241)
O$_2$—H$_t$	—	—	—	—	—
	(0.3561)	(−2.4914)	(1.6942)	(0.1908)	(−0.6907)
C—H$_m$	0.2718	−0.8967	1.4196	0.1619	−0.2682
	(0.2723)	(−0.9002)	(1.4022)	(0.1569)	(−0.2678)
C—H$_a$	0.2736	−0.9083	1.4061	0.1539	−0.2692
	(0.2723)	(−0.8993)	(1.4149)	(0.1571)	(−0.2676)
O$_1$—H$_a$	0.0040	0.0129	0.1710	0.6750	0.0005
	(0.0018)	(0.0065)	(0.1428)	(0.6691)	(0.0004)
C—H$_t$	—	—	—	—	—
	(0.0073)	(0.0280)	(0.1547)	(0.7109)	(0.0018)

^{a} See Method and calculation details for an explanation of symbols. ^{b} See Figure 4 for atom labels. ^{c} T is Si$_2$ in **3**. T is Al in **4**.

The topological properties calculated at the BCP's of the electronic density for complexes **3** and **4** are summarized in Table 3. It can be seen that no important changes occur in clusters **1** and **2** after the interaction with methane. On the other hand, the topological properties of methane in complexes **3** and **4** are characteristic of shared interactions. Moreover, those properties show very small changes with respect to their values in the isolated molecule.[30] The most important bonds to analyze within the AIM theory are obviously O$_1$—H$_a$ and C—H$_t$. In particular, the attention is focused on ρ_b and $\nabla^2\rho_b$, and their comparison with the reference values of 0.002−0.034 and 0.024−0.139 au, respectively, given by Koch and Popelier to help in the characterization of a given bond as a hydrogen bond.[28] Thus, it can be seen that both ρ_b and $\nabla^2\rho_b$ at the C—H$_t$ bond are within the reference values. In the case of the O$_1$—H$_a$ bond in complex **3**, the value of $\nabla^2\rho_b$ is outside the above range, whereas for the O$_1$—H$_a$ bond in complex **4**, both ρ_b and $\nabla^2\rho_b$ are outside the reference ranges. Then, the application of those two criteria indicate that the O$_1$—H$_a$ bonds cannot be classified as hydrogen bonds on the basis of the AIM theory and must be characterized as van der Waals interactions, whereas the C—H$_t$ bond fulfils the above criteria to be designated as a weak hydrogen bond.

Figures 5 and 6 depict the $\nabla^2\rho(\mathbf{r})$ contour maps for structures **3** and **4**. No appreciable changes can be observed when those figures are compared with the contour maps corresponding to the isolated clusters, Figures 2 and 3, respectively. It can also be seen in both figures that the bond paths beginning at the BCP between O$_1$ and H$_a$ on one hand, and between C and H$_t$ on the other hand, conclude in those nuclei, this being a necessary condition for the existence of a hydrogen bond.[28]

Table 4 lists several other properties that could help in the proper characterization of the O$_1$—H$_a$ and C—H$_t$ bonds and then could be useful to understand the change in the chemical reactivity of a zeolite when it undergoes an isomorphic substitution.

The bonded and van der Waals nonbonded radii of the atoms involved in the O$_1$—H$_a$ and C—H$_t$ bonds in complexes **3** and **4** are given in Table 4. Their respective penetrations and the mutual penetration are shown as well. Koch and Popelier stated
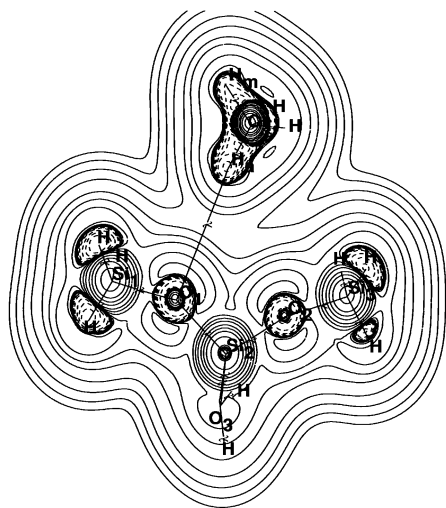
Effect of Si → Al Substitution on the Zeolite Structure

J. Phys. Chem. A, Vol. 107, No. 32, 2003 **6229**

Figure 5. Laplacian of the electronic charge density of structure **3**. The plane containing the O_1–H_a–C atoms is shown. Broken lines represent regions of electronic charge concentration and solid lines denote regions of electronic charge depletion. BCP are indicated with black circles. The molecular graph is also indicated.
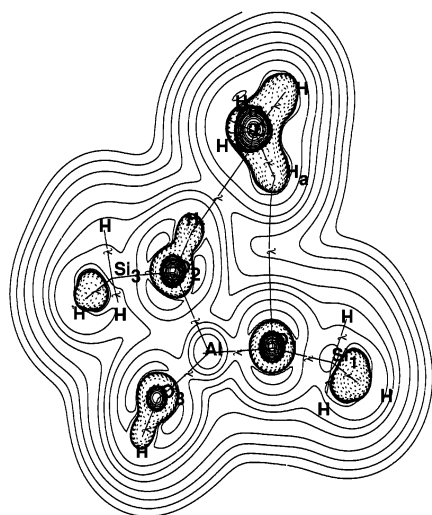

Figure 6. Laplacian of the electronic charge density of structure **4**. The plane containing the O_1–H_a–C atoms is shown. Broken lines represent regions of electronic charge concentration and solid lines denote regions of electronic charge depletion. BCP are indicated with black circles. The molecular graph is also indicated.

as a necessary condition for a hydrogen bond to exist that the mutual penetration of the atoms involved in the bond must be positive and, furthermore, the hydrogen atom must be more penetrated than the base atom.[28] Table 4 clearly shows that the individual penetrations and the mutual penetrations are negative in all cases, with the only exception of atom H_a in complex **3**, which exhibits a slightly positive penetration. Thus, according to the above authors these bonds could not be characterized as hydrogen bonds, but they could be described as weak van der Waals interactions instead.

Another necessary condition to characterize a bond as a hydrogen bond is the loss of charge undergone by the hydrogen atom involved in it.[28] The loss of charge can be calculated by subtracting the average number of electrons of the hydrogen atom, $N(H)$, in the isolated methane molecule or in the isolated zeolite from the corresponding value in the complex. It can be seen from Table 4 that $\Delta N(H)$ is negative in all cases, thus fulfilling the above criterion to define a given bond as a

TABLE 4: Nonbonded and Bonded Radii, Penetration, and Mutual Penetration of Atoms H_a, O_1, H_t, and C in Complexes 3 and 4, and the Change in the Average Number of Electrons, Atomic Energy, Dipolar Polarization, and Atomic Volume of Atoms H_a and H_t after the Interaction of Methane with Structures 1 and 2 To Give Rise to Complexes 3 and 4[a]

| property[b] | 3 | | 4 | | | |
	H_a	O_1	H_a	O_1	H_t	C
r°_X	2.31	3.14	2.31	3.28	1.70	2.73
r_X	2.23	3.27	2.72	3.73	1.74	3.07
Δr_X	0.08	−0.13	−0.41	−0.45	−0.04	−0.34
$\Sigma \Delta r_X$	−0.05		−0.86		−0.38	

| change in the property[b] | 3 | 4 | |
	H_a	H_a	H_t
$\Delta N(H)$	−0.023	−0.016	−0.003
$\Delta E(H)$	0.013	0.010	0.004
$\Delta |M(H)|$	−0.020	−0.013	−0.009
$\Delta V(H)$	−0.066	−0.298	−1.016

[a] See Method and calculation details for an explanation of symbols.
[b] All properties are given in au.

hydrogen one. It should be noted, however, that the $\Delta N(H)$ values reported in Table 4 are smaller than the values given in Table 7 of ref 28 for bonds that were classified as weak van der Waals interactions.

The formation of a hydrogen bond is also responsible for the energetic destabilization and the decrease of the dipolar polarization of the hydrogen atom involved in that bond.[28] Thus, these criteria could help to further characterize the interactions found in complexes **3** and **4**.

The energy destabilization of the hydrogen atom, $\Delta E(H)$, is calculated as the difference in its atomic energy in the complex and in the isolated monomer. By its definition, this quantity must be positive. It can be seen in Table 4 that an energetic destabilization of the H_a and H_t atoms occur in both complexes.

The reduction of the dipolar polarization of the hydrogen atom, $\Delta |M(H)|$, is computed by subtracting $|M(H)|$ in the isolated monomer from the corresponding value in the complex. It is observed in Table 4 that a decrease in the dipolar polarization of the H_a and H_t atoms take place after the formation of complexes **3** and **4**.

Finally, a last criterion to evaluate the existence of a hydrogen bond is associated with a decrease in the atomic volume of the hydrogen atom, $V(H)$, after the complex is formed. As can be seen from Table 4, a decrease of the atomic volume of both H atoms occur for both complexes. It is worth noting, nevertheless, that the observed $\Delta V(H)$ values are smaller or slightly smaller than the values reported in Table 10 of ref 28 for those bonds that were described as weak van der Waals interactions.

In summary, it can be said that the O_1–H_a bonds fail to fulfill several of the above criteria so as to be classified as hydrogen bonds. On the other hand, the C–H_t bond fails to satisfy the mutual penetration, the loss of charge, and the decrease of the atomic volume criteria. Taking those facts into account, it is safe to state that methane interacts with a zeolite through a very weak Si–O···H–C van der Waals interaction before the isomorphic substitution of Si by Al takes place. When the isomorphic substitution occurs, the interaction of methane with the zeolite takes place through a weak O–H···C van der Waals interaction involving the Brønsted acid site of the zeolitic system. These findings clearly disagree with those of Benco et al. who claim that the adsorption of linear hydrocarbons on zeolites occurs via the formation of hydrogen bonds.[4]

Conclusions

The isomorphic substitution of silicon by aluminum in a zeolite cluster was investigated in this work within the framework of the density functional and the atoms-in-molecules theories to get a deeper understanding into the effects of aluminum on the zeolite structure. Furthermore, the interaction of methane with those clusters was also studied as a further step toward the understanding of the influence of the isomorphic substitution over the adsorption of hydrocarbons on zeolites.

The effect of the substitution of silicon by aluminum in a zeolite cluster is 2-fold. As a consequence of the different formal ionic charge of the aluminum ion with respect to the silicon one, hydroxyl groups appear to preserve the electric neutrality of the whole zeolitic system. Those hydroxyl groups represent acid sites according to their topological properties and give rise to the well-known Brønsted acid sites. On the other hand, those oxygen atoms not involved in the acid sites show an slight increase in their base character.

The calculated interaction energy for the adsorption of methane over the zeolite clusters indicates that the hydrocarbon interacts weakly with the zeolite after the isomorphic substitution takes place. On the other hand, there is no appreciable stabilization before the isomorphic substitution occurs.

The calculated topological properties for the two adsorption complexes mentioned above clearly show that the interaction of methane with the zeolite cluster before the isomorphic substitution takes place through the formation of a weak van der Waals interaction between a nonprotonated oxygen atom of the zeolite and a hydrogen atom of methane. After the substitution of silicon by aluminum occurs the interaction of methane with the zeolite takes place mainly via the formation of a weak van der Waals interaction between the Brønsted acid site of the zeolite and the carbon atom of methane.

In summary, it is argued that the isomorphic substitution of silicon by aluminum in a zeolite cluster develops a Brønsted acid site and this fact would be responsible for the stabilization undergone by methane when it interacts with the substituted zeolite.

References and Notes

(1) van Santen, R. A.; Kramer, G. J. *Chem. Rev.* **1995**, *95*, 637.

(2) Sauer, J.; Ugliengo, P.; Garrone, E.; Saunders: V. R. *Chem. Rev.* **1994**, *94*, 2095.

(3) Okulik, N. B.; Pis Diez, R.; Jubert, A. H.; Esteves, P. M.; Mota, C. J. A. *J. Phys. Chem. A* **2001**, *105*, 7079.

(4) Benco, L.; Demuth, T.; Hafner, J.; Hutschka, F.; Toulhoat, H. *J. Chem. Phys.* **2001**, *114*, 6327.

(5) Viruela, P.; Zicovich-Wilson, C. M.; Corma, A. *J. Phys. Chem.* **1993**, *97*, 13713.

(6) Zicovich-Wilson, C. M.; Viruela, P.; Corma, A. *J. Phys. Chem.* **1995**, *99*, 13224.

(7) Blaszkowski, S. R.; van Santen, R. A. *Top. Catal.* **1997**, *4*, 145.

(8) Soscún, H.; Hernández, J.; Castellano, O.; Díaz, G.; Hinchliffe, A. *Int. J. Quantum Chem.* **1998**, *70*, 951.

(9) Sinclair, P. E.; Catlow, C. R. A. *Faraday Trans.* **1997**, *93*, 333.

(10) van Santen, R. A. *Catal. Today* **1997**, *38*, 377.

(11) Boronat, M.; Viruela, P.; Corma, A. *J. Phys. Chem. A* **1998**, *102*, 982.

(12) Sauer, J. *J. Chem. Rev.* **1989**, *89*, 199.

(13) Blaszkowski, S. R.; van Santen, R. A. *J. Phys. Chem. B* **1997**, *101*, 2292.

(14) Frash, M. V.; Kazansky, V. B.; Rigby, A. M.; van Santen, R. A. *J. Phys. Chem. B* **1997**, *101*, 5346.

(15) (a) Hohenberg, P.; Kohn, W. *Phys. Rev.* **1964**, *136B*, 864. (b) Kohn, W.; Sham, L. J. *Phys. Rev.* **1965**, *140A*, 1133. (c) Parr, R. G.; Yang, W. *Density Functional Theory of Atoms and Molecules*; Oxford University Press: Oxford, U.K., 1989.

(16) Eder, F.; Lercher, J. A. *J. Phys. Chem. B* **1997**, *101*, 1273.

(17) (a) Parillo, D. J.; Gorte, R. J. *J. Phys. Chem.* **1993**, *97*, 8786. (b) Greatbanks, S. P.; Hillier, I. H.; Burton, N. A. *J. Chem. Phys.* **1996**, *105*, 3770.

(18) Bader, R. F. W. *Atoms in Molecules—A Quantum Theory*; Clarendon Press: Oxford, U.K., 1990.

(19) Eichler, U.; Brändle, M.; Sauer, J. *J. Phys. Chem. B* **1997**, *101*, 10035.

(20) Becke, A. D. *J. Chem. Phys.* **1993**, *98*, 5648.

(21) Lee, C.; Yang, W.; Parr, R. G. *Phys. Rev. B* **1988**, *37*, 785.

(22) Frisch, M. J.; Trucks, G. W.; Schlegel, H. B.; Scuseria, G. E.; Robb, M. A.; Cheeseman, J. R.; Zakrzewski, V. G.; Montgomery, J. A., Jr.; Stratmann, R. E.; Burant, J. C.; Dapprich, S.; Millam, J. M.; Daniels, A. D.; Kudin, K. N.; Strain, M. C.; Farkas, O.; Tomasi, J.; Barone, V.; Cossi, M.; Cammi, R.; Mennucci, B.; Pomelli, C.; Adamo, C.; Clifford, S.; Ochterski. J.; Petersson, G. A.; Ayala, P. Y.; Cui, Q.; Morokuma, K.; Malick, D. K.; Rabuck, A. D.; Raghavachari, K.; Foresman, J. B.; Cioslowski, J.; Ortiz, J. V.; Baboul, A. G.; Stefanov, B. B.; Liu, G.; Liashenko, A.; Piskorz, P.; Komaromi, I.; Gomperts, R.; Martin, R. L.; Fox, D. J.; Keith, T.; Al-Laham, M. A.; Peng, C. Y.; Nanayakkara, A.; Gonzalez, C.; Challacombe, M.; Gill, P. M. W.; Johnson, B.; Chen, W.; Wong, M. W.; Andres, J. L.; Gonzalez, C.; Head-Gordon, M.; Replogle, E. S.; Pople, J. A. *Gaussian 98*, revision A.7; Gaussian, Inc.: Pittsburgh, PA, 1998.

(23) Boys, S. F.; Bernardi, F. *Mol. Phys.* **1970**, *19*, 553.

(24) Blieger-Konig, W.; Bader, R. F. W.; Tang, T. H. *J. Comput. Chem.* **1982**, *3*, 317.

(25) Bader, R. F. W. *J. Phys. Chem. A* **1998**, *102*, 7314.

(26) (a) Bader, R. F. W.; Beddall, P. M.; Cade, P. E. *J. Am. Chem. Soc.* **1971**, *93*, 3095. (b) Bader, R. F. W.; Preston, H. J. *Theor. Chim. Acta* **1970**, *17*, 384. (c) Bader, R. F. W.; Carroll, M. T.; Cheeseman, J. R.; Chang, C. *J. Am. Chem. Soc.* **1987**, *109*, 7968.

(27) Carroll, M. T.; Bader, R. F. W. *Mol. Phys.* **1988**, *65*, 695.

(28) Koch, U.; Popelier, P. L. A. *J. Phys. Chem.* **1995**, *99*, 9747.

(29) The C—H bonds and the H—C—H angles are found to be 1.092 Å and 109.5°, respectively, in isolated methane. The calculations are accomplished at the B3LYP/6-31G** level of theory.

(30) The density at the BCP, ρ_b, and its corresponding Laplacian, $\nabla^2\rho_b$, amounts to $+0.2716$ and -0.8959 au, respectively, in isolated methane.